Environmental Science & Technology

pubs.acs.org/est

Article

Solubility and Thermodynamic Investigation of Meta-Autunite Group Uranyl Arsenate Solids with Monovalent Cations Na and K

Isabel Meza, Jorge Gonzalez-Estrella, Peter C. Burns, Virginia Rodriguez, Carmen A. Velasco, Ginger E. Sigmon, Jennifer E. S. Szymanowski, Tori Z. Forbes, Lindsey M. Applegate, Abdul-Mehdi S. Ali, Peter Lichtner, and José M. Cerrato*

Cite This: *Environ. Sci. Technol.* 2023, 57, 255−265

Read Online

ACCESS | Metrics & More | Article Recommendations | Supporting Information

ABSTRACT: We investigated the aqueous solubility and thermodynamic properties of two meta-autunite group uranyl arsenate solids (UAs). The measured solubility products (log K_{sp}) obtained in dissolution and precipitation experiments at equilibrium pH 2 and 3 for NaUAs and KUAs ranged from −23.50 to −22.96 and −23.87 to −23.38, respectively. The secondary phases $(UO_2)(H_2AsO_4)_2(H_2O)_{(s)}$ and trögerite, $(UO_2)_3(AsO_4)_2 \cdot 12H_2O_{(s)}$, were identified by powder X-ray diffraction in the reacted solids of KUA precipitation experiments (pH 2) and NaUAs dissolution and precipitation experiments (pH 3), respectively. The identification of these secondary phases in reacted solids suggest that H_3O^+ co-occurring with Na or K in the interlayer region can influence the solubilities of uranyl arsenate solids. The standard-state enthalpy of formation from the elements ($\Delta H_{f\text{-el}}$) of NaUAs is −3025 ± 22 kJ mol^{-1} and for KUAs is −3000 ± 28 kJ mol^{-1} derived from measurements by drop solution calorimetry, consistent with values reported in other studies for uranyl phosphate solids. This work provides novel thermodynamic information for reactive transport models to interpret and predict the influence of uranyl arsenate solids on soluble concentrations of U and As in contaminated waters affected by mining legacy and other anthropogenic activities.

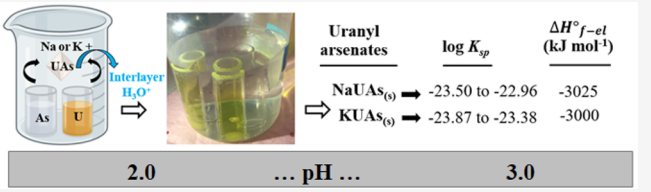

KEYWORDS: *uranyl, arsenate, solubility, thermodynamic, interlayer cation*

INTRODUCTION

The chemical behaviors of uranyl arsenate solids (UAs) are important because they are found within uranium (U) mining operations and have been noted as co-occurring contaminants within drinking water sources.[1−6] Communities near these sites can be impacted by the releases of U and arsenic (As), which are of major concerns for public health as both are toxic and carcinogenic.[7−9] Minerals containing U and As occur in the major uranium mines in Key Lake, Saskatchewan, Canada, St. Austell District of Cornwall, England, and in several southwestern U.S. sites.[5,10−12] Even in areas that are not impacted by mining operations, U and As can co-occur naturally in waters and soils in community lands. For instance, the spatial relationship between U and As in the Northern Plains was evaluated, and both elements were found at elevated concentrations in the groundwater in three inhabited regions in North Dakota and South Dakota.[4,13] Also, it was noted that there was a spatial correlation of groundwater containing U and As associated with a flow along a geologic contact; however, the underlying mechanisms enabling the U and As correlation warrant further study.[4,14] Native American communities near these sites are concerned about the releases of toxic U and As levels in their water sources.[6,11,15] Therefore, it is crucial to develop a greater understanding of UAs and their behavior in natural waters.

Uranyl arsenates are one of the most diverse chemical groups of U minerals but are less characterized than the related phosphate phases.[16−18] Currently, the International Mineralogical Association lists 36 mineral species that contain both essential U and As.[19] Arsenates and phosphates populate the meta-autunite group ($A^{n+}[(UO_2)(TO_4)](H_2O)$), where A^{n+} is a mono-, di-, or trivalent cation; T = P, As) with the same structural topology.[20] This group of minerals contains uranyl ions $[(UO_2)^{2+}]$ in square bipyramidal polyhedra linked through equatorial corner-sharing with phosphate or arsenate tetrahedra.[21] This unit then links to neighboring UO_2^{2+} cations to form a 2-D sheet, and charge balancing cations [i.e., sodium (Na^+), potassium (K^+), calcium (Ca^{2+})] and water molecules are located between the U(VI) layers to form the final 3-D crystalline lattice.[18,22] Arsenate and phosphate-bearing anionic units are generally isostructural, have similar sizes and charges, precipitate as uranyl minerals at elevated concentrations, and

Received: September 11, 2022
Revised: November 29, 2022
Accepted: November 30, 2022
Published: December 16, 2022

form ternary complexes on surfaces at low concentrations.[23−26] Uranyl phosphates have generally low solubilities ranging from log K_{sp} of −13.17 for uranyl hydrogen phosphate to −49.36 and −50.39 for uranyl orthophosphate.[16,25,27] The solubility of $(UO_2)_3(AsO_4)_2{\cdot}12H_2O$ has been previously measured, but only within heterogeneous water−salt systems,[25,28] and thus, these solubility measurements should be confirmed under both supersaturation and undersaturation.[29,30] These previous studies indicate that the thermodynamics of UAs need more documentation.[25,28,31,32]

Moreover, there is incomplete information about the thermodynamic values for UAs containing alkali or alkali-earth cations.[18,25,28] The formation of U−As−Ca precipitates has been identified at acidic pH and that bicarbonate facilitates the dissolution of U-, As-, and Ca-bearing solids at circum-neutral pH.[33] A previous study by Dzik et al.[18] provided calorimetry measurements for UAs of the meta-autunite group containing K^+, lithium (Li^+), cesium (Cs^+), strontium (Sr^{2+}), and copper (Cu^{2+}) but did not provide solubility values. Additionally, the role of H^+ in the form of hydronium (H_3O^+) substituted with monovalent cations in meta-autunite UAs remains poorly understood.

The objective of this study was to determine the solubility and thermodynamic properties of two uranyl arsenate phases: sodium uranyl arsenate $(Na_{0.5}(H_3O)_{0.5}[(UO_2)(AsO_4)]\text{-}(H_2O)_{2.5(s)}$ (NaUAs) and potassium uranyl arsenate $K_{0.9}[(H_3O)_{0.1}(UO_2)(AsO_4)](H_2O)_{2.5(s)}$ (KUAs). While the inclusion of cations (e.g., Na^+, K^+, Ca^{2+}) in the interlayer region of meta-autunite UAs is widely documented,[18,28,34,35] our understanding on how this substitution affects the solubility of uranyl arsenate solids remains limited. The novelty of this investigation is the identification of the impact of monovalent cations such as Na^+, K^+, and H_3O^+ on the solubilities of UAs at acidic pH using various aqueous chemistries, solid-state chemistries, thermodynamic techniques, and speciation calculations. The knowledge generated from this study contributes to improve our understanding of U and As mobilities in the environment, expanding on the limited existing data related to the solubilities of uranyl arsenate solids and minerals. This information can consequently contribute to a reliable and internally consistent database that can be applied in reactive transport models.

MATERIALS AND METHODS

Synthesis. Uranyl arsenate solids (NaUAs and KUAs) were synthesized at room temperature over the course of one to two weeks by the diffusion method which allowed a slow mixing of reactants emerging from two vials inside of a barrier solution in a beaker as described by Dzik et al.[16] This method is known for providing high quality, purity, and yield of the material required for calorimetric measurements. Additional details describing this synthesis process are included in the Supporting Information (see additional Materials and Methods and Table S1).

Analytical Methods. Powder X-ray diffraction (p-XRD), electron microprobe analysis, scanning electron microscopy (SEM), energy dispersive X-ray spectroscopy (EDS), and thermogravimetric analyses (TGA) were used to characterize the unreacted and reacted solids. The soluble concentrations of U, As, Na, and K in aqueous solutions were measured using inductively coupled plasma optical emission spectrometry (ICP-OES) and inductively coupled plasma mass spectrometry (ICP-MS). Acid digestions (∼1 mL of nitric acid and 2 mL of hydrochloric acid) were conducted by heating in a Digi prep MS SCP Science block digester at 90 °C for 2 h to assess the acid extractable elements from the synthesized solids. Additional details describing the solution analyses are included in the Supporting Information. Additional details describing the solid analyses are included in the Supporting Information (Texts S1−S3).

Solubility Experiments. All solubility experiments were conducted in triplicate at pH 2 and 3 at 25 °C in batch reactors (Teflon Nalgene bottles) using a UA solid to water mass ratio of 1.4 (i.e., ∼40 mg of UAs in 28 mL of 18 MΩ H2O) for 31 days (d) reaction time. Batch reactors were sealed and agitated at 60 rpm in an analog rotisserie tube rotator (Scologex MX-RL-E, Rocky Hill, CT, US) for the duration of the experiment. Each experimental reactor solution was initially adjusted to the targeted pH 2 or 3 using small quantities of concentrated HNO_3 and monitored daily using a pH microelectrode (Thermo Orion Ross) calibrated with 3 NIST standard solutions (pH 4, 7, and 10); no further adjustment was necessary during the 31 d reaction time. The pH range from 2 to 3 was chosen because the chemical speciation of U and As is well constrained at low pH. For example, chemical equilibrium modeling indicates that UO_2^{2+} is the predominant species of U, while H_3AsO_4 and $H_2AsO_4^{1-}$ are the predominant species of As with limited influence of the carbonate system (i.e., carbonic acid is predominant at this acidic pH). We attempted to make a solution at pH 4, but the pH stabilized in the proximity of 3, so we decided to stay in the acidic range from 2 to 3.

Two types of experiments were performed to accurately evaluate the solubilities of the NaUAs and KUAs solids. The first type was a dissolution experiment whereby UAs (NaUAs or KUAs) were added first to the vial and then the 18 MΩ H_2O. The second type was a precipitation experiment where besides the UAs and 18 MΩ H_2O, Na or K, As, and U were added as $NaNO_3$ or KNO_3, $(NO_3)_2(H_2O)_6$, As_2O_5, and UO_2, respectively, in that order. For the precipitation experiments carried out at pH 2, the initial concentrations were ∼2.7 mM of U, As, and Na for the assays amended with NaUAs and ∼2.5 mM of U, As, and K for the assays amended with KUAs. Chemical equilibrium modeling determined higher saturation indices at pH 3 compared to those obtained at pH 2. Thus, for the precipitation experiments carried out at pH 3, the initial concentrations were ∼1.5 mM of U, As, Na, and K for the assays amended either with NaUAs and KUAs. We determined that precipitation occurred if at least one of the final concentrations of U, As, or Na decreased from the starting values.

Throughout the two different types of experiments, batch reactors were sealed and agitated at 60 rpm in an analog rotisserie tube rotator (Scologex MX-RL-E, Rocky Hill, CT, US) at room temperature. Aliquots of the solution were extracted at various times (0 min, 15 min, 30 min, 60 min, 120 min, 4 h, 6 h, 8 h, 12 h, 24 h, 8 d, 15 d, 22 d, 31 d), filtered through 0.1 μm MilliporeSigma Millex filters, and diluted for ICP-OES or MS analyses to determine dissolved concentrations of U, As, and Na or K. One control reactor, where only one aliquot was withdrawn at day 31, was used to validate that sampling during the experimental period did not significantly change the dissolved element concentrations. To verify the composition of the remaining solid at the end of each experiment, ∼20 mg of reacted material was collected for p-

https://doi.org/10.1021/acs.est.2c06648
Environ. Sci. Technol. 2023, 57, 255−265

Table 1. Reaction Stoichiometry for Uranyl Arsenate Solids Considered in the Thermodynamic Modeling Conducted in This Study[a]

Experimental pH	Solid phase	Mass action equation[b]	Log K_{sp} at dissolution	Log K_{sp} at precipitation
2	NaUAs	$K_{sp} = a(UO_2)^{2+} \cdot a(AsO_4)^{3-} \cdot a^{0.5}(H_3O)^{+} \cdot a^{0.5}Na^{+}$	−23.50	−22.96
3	NaUAs		−23.15	−23.15
	+			
	Trögerite $(UO_2)_3(AsO_4)_2{\cdot}12H_2O_{(s)}$	$K_{sp} = a(UO_2)^{2+} \cdot a(AsO_4)^{3-}$	−47.97	−48.85
			−45.33[c]	−
2	KUAs	$K_{sp} = a(UO_2)^{2+} \cdot a(AsO_4)^{3-} \cdot a^{0.1}(H_3O)^{+} \cdot a^{0.9}K^{+}$	−23.87	−23.50
	+			
	$(UO_2)(H_2AsO_4)_2(H_2O)$	$K_{sp} = a(UO_2)^{2+} \cdot a^{2}(AsO_4)^{3-} \cdot a^{-4}H^{+}$	−47.19	−46.97
3	KUAs	$K_{sp} = a(UO_2)^{2+} \cdot a(AsO_4)^{3-} \cdot a^{0.1}(H_3O)^{+} \cdot a^{0.9}K^{+}$	−23.57	−23.38

[a]All the calculations of log K_{sp} values consider uranyl−arsenate complexes. [b]The following reactions are provided as examples: For NaUAs: $Na_{0.5}(H_3O)_{0.5}(UO_2)(AsO_4)(H_2O)_{2.5(s)} \leftrightarrow (AsO_4)^{3-} + UO_2^{2+} + 0.5Na^{+} + 0.5(H_3O)^{+} + 2.5H_2O$. For KUAs: $K_{0.9}(H_3O)_{0.1}(UO_2)(AsO_4)(H_2O)_{2.5(s)} \leftrightarrow (AsO_4)^{3-} + (UO_2)^{2+} + 0.9K^{+} + 0.1(H_3O)^{+} + 2.5H_2O$. For trögerite $(UO_2)_3(AsO_4)_2 \cdot 12H_2O_{(s)}$: $(UO_2)_3(AsO_4)_2 \cdot 12H_2O_{(s)} \leftrightarrow 2(AsO_4)^{3-} + 3(UO_2)^{2+} + 12H_2O$. For $(UO_2)(H_2AsO_4)_2(H_2O)$: $(UO_2)(H_2AsO_4)_2(H_2O)_{(s)} \leftrightarrow 2(AsO_4)^{3-} + (UO_2)^{2+} + H_2O + 4H^{+}$. [c]log K_{sp} obtained by Nipruk et al.[25]

XRD (Figure S1) and SEM analyses of reacted solid samples (Figure S2).

Thermodynamic Modeling. Calculations were carried out using the open-source computer code PFLOTRAN that runs on MacOSX, Linux, and Windows.[36] PFLOTRAN applies the law of mass action to obtain the aqueous species complexes as a function of the free ion concentrations. Table 1 shows the reaction stoichiometry used for each uranyl arsenate solid in the log K_{sp} calculations. Solubility product calculations were only performed using data points that corresponded to samples taken from each batch reactor after they had achieved equilibrium. The concentrations at equilibrium were obtained using average values calculated over a ± 10% interval during 31 d (Table S2). Once the dissolution and precipitation experiments were completed, we were able to verify if equilibrium was reached in these experiments. This equilibrium was verified using the log K_{sp} for the dissolution experiments with the concentrations of the precipitation experiments and comparing the saturation index (SI) obtained with the precipitation experiment, which was lower than 1 in all cases (Tables S6 and S7). The measured U, As, Na, and K concentrations and pH values at equilibrium used for the log K_{sp} speciation calculations are listed in the Table S2. Table S3 shows the speciation equations and thermodynamic relations that are described below in detail. For each solubility value, we calculated the ionic strength of the solution (I) using Table S3, eq 5, in the SI. We used the Debye−Hückel algorithm to correct the concentrations (valid for ionic strength lower than 0.1 M) described in Table S3, eq 6, in the SI.

To obtain the log K_{sp} we used Table S3, eq 4, in the SI, and the mineral law of mass action equation, a function of the free ion concentrations of the primary species including the pH. From the experimental total concentrations (from solubility experiments) at equilibrium (C_j^{tot}) using Table S3, eq 3, we obtained the primary (C_j) and secondary (C_i) species concentrations. Then, using the mass action eq (Table S3, eq 4, in SI) corresponding to the concentrations obtained from a speciation calculation, the saturation index (SI) was calculated (Table S3, eq 8, in SI). From the value obtained for the SI, we subsequently adjusted the solubility product constant (log K_{sp}) by the log SI so that the log SI = 0 was achieved (log K_{sp} = log K_{sp} − log SI). The process of adjusting the log K_{sp} value consisted of changing the database log K_{sp} until we get a SI equal to zero.

Standard states used in this research for solid phases and for H_2O are the pure mineral or fluid at the temperature and pressure of the experiments. Molal activity coefficients of neutral aqueous species are assumed to be unity. The thermodynamic database (Thermochemie V10a.dat)[37] used by PFLOTRAN was expanded to include K_{sp} values from Gorman-Lewis et al.[30] and from Nipruk et al.[25] and includes the most recent update to U aqueous complexes, for example, those presented in Rutsch et al.: $UO_2H_2AsO_4^{+}$, $UO_2(H_2AsO_4)_2$, and UO_2HAsO_4 (Table S4).[31,38−41]

High-Temperature Oxide-Melt Calorimetry. A Setaram Alexsys high-temperature oxide-melt calorimeter was used to measure drop solution enthalpies of NaUAs and KUAs. Calorimetric techniques and experimental details can be found in the existing literature.[42−45] The calorimeter was calibrated using the heat content of Al_2O_3. The calorimeter was flushed with high purity O_2 for the duration of the experiment to remove moisture from the environment. The samples were initially ground and then pressed into ∼5 mg pellets and accurately weighed before the drop. The pellets were then dropped from room temperature into the calorimeter, which contained a sodium molybdate ($3Na_2O{\cdot}4MO_3$) solvent that was equilibrated at 976 K. Each experiment was performed over the course of approximately 75 min, and the experiments for which the baseline stabilized after collection were used for data analysis. Enthalpy of the drop solution (ΔH_{ds}) was obtained as an average of each experiment. Thermocycles were then used to calculate the enthalpies of formation of both the oxide and element species.

The calculated log K_{sp} value for each uranyl arsenate solid was used to determine the state Gibbs free energy of formation (ΔG_f)) starting with the standard state Gibbs free energy of reaction ΔG_r) for each dissolution reaction of interest (Table S3, eqs 9 and 10, in SI). Using the enthalpies of formation from elements ($\Delta H_{f\text{-el}}$) and ΔG_f, the standard-state entropy of formation (ΔS_f) can be calculated (Table S3, eq 11, in SI). The ΔS_f was obtained using Table S3 in SI with the $\Delta H_{f\text{-el}}$[27] and with the values obtained from Cox et al.[46] and Nordstrom et al.[47] that are $\Delta G^{\circ}_{f(H_2O)}$= −237.14; $\Delta G^{\circ}_{f(UO_2^{2+})}$= −952.55; $\Delta G^{\circ}_{f(AsO_4^{3-})}$ = −646.36; $\Delta G_{f_{(Na^{+})}}$ = −261.95 in kJ mol^{-1}.

RESULTS AND DISCUSSION

Stoichiometries of NaUAs and KUAs. The p-XRD diffraction patterns of NaUAs and KUAs exhibit sharp profiles,

https://doi.org/10.1021/acs.est.2c06648
Environ. Sci. Technol. 2023, 57, 255−265

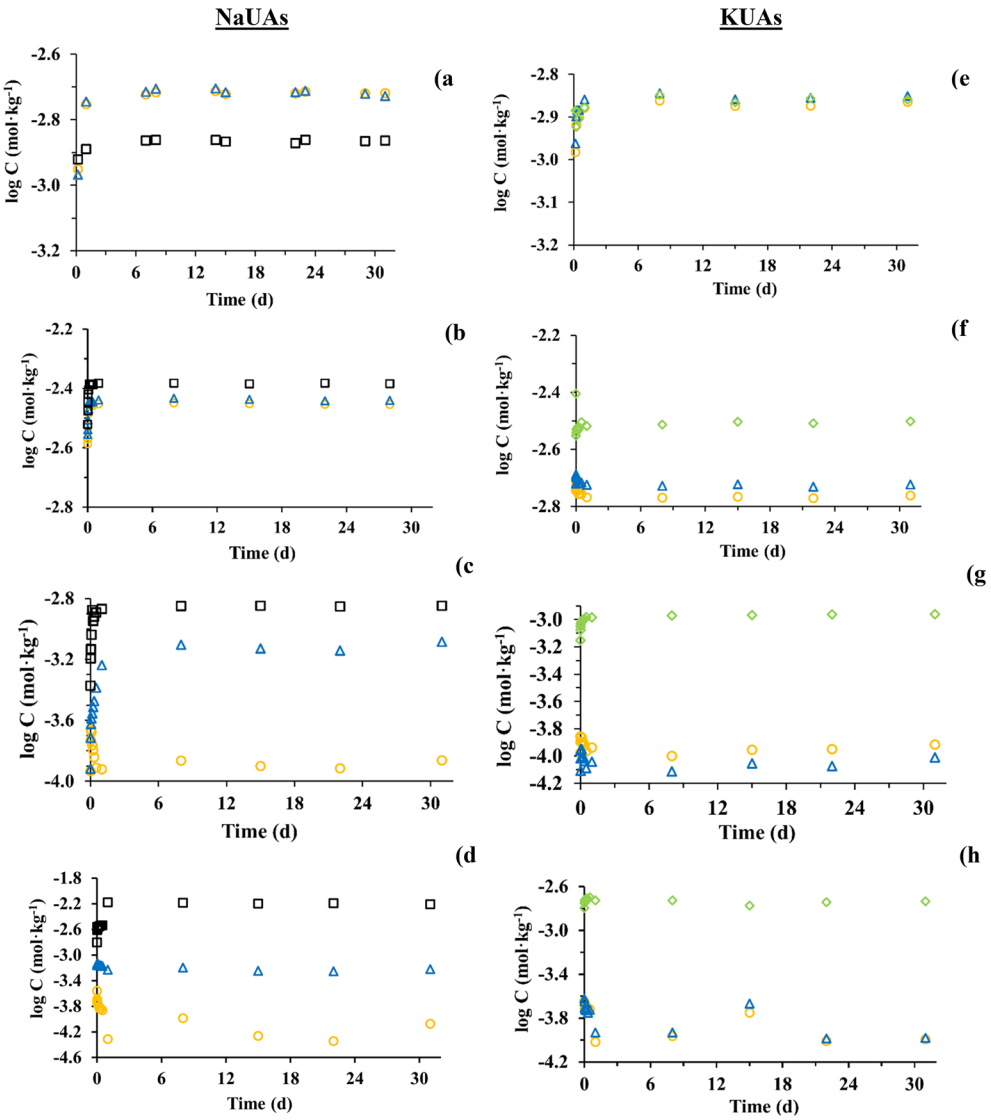

Figure 1. Experimental measurements of the dissolved concentrations of U (circles), As (triangles), Na (squares), and K (diamonds) as log mol·kg^{-1} against time for NaUAs for dissolution (a) and precipitation experiments (b) at pH 2 and dissolution (c) and precipitation experiments (d) at pH 3 and for KUAs for dissolution (e) and precipitation experiments (f) at pH 2 and dissolution (g) and precipitation experiments (h) at pH 3.

and all peaks are assignable to the target phase, confirming the identities of NaUAs and KUAs (Figure S1). The mass loss over 30−170 °C of 9% was attributed to the water contained in each compound (Figure S3) by TGA, which represents ∼2.5 mol of water (H_2O) and agrees with the molecular formulas of the NaUAs and KUAs. Chemical analyses for acid digestions of NaUAs and KUAs using ICP-OES indicate U:As molar ratios near 1 as expected. However, deficiencies in the alkali cation content relative to the end-member formula (Table S5) were detected. Spatially resolved analyses using electron microprobes (Table S5) confirmed the deficiencies of alkali cation concentrations relative to the end-member compositions. The derived compositions are

$$\text{NaUAs} = Na_{0.5}(H_3O)_{0.5}[(UO_2)(AsO_4)](H_2O)_{2.5(s)}$$

$$\text{KUAs} = K_{0.9}(H_3O)_{0.1}[(UO_2)(AsO_4)](H_2O)_{2.5(s)}$$

Chemical analyses, p-XRD, and microscopy (Table S5, Figure S1 and Figure S2) indicated that single phases of NaUAs and KUAs were obtained using the diffusion method described in the Materials and Methods section. Single phase crystals of uranyl arsenates of the meta-autunite group with mono and divalent cations have also been identified in previous studies after synthesis using the same method.[18,34] The discrepancy between the cation's concentration with the microprobe and acid digestion analyses for KUAs is attributed to instability of the compound during electron beam irradiation, as is typical for similar compounds under the microprobe beam.[48]

The chemical analyses of both compounds NaUAs and KUAs indicate that H_3O^+ is present with K^+ or Na^+ in the interlayer region of the structures. The hydronium-bearing uranyl arsenate analog of uranospinite, $(H_3O)_2[(UO_2)_2(AsO_4)_2](H_2O)_8$, has been documented.[46] Chernikovite is a well-characterized H_3O^+-bearing autunite-structure compound with composition $(H_3O)_2[(UO_2)_2(PO_4)_2](H_2O)_n$, and a hydronium-$K^+$ solid-solution series has been noted in this uranyl phosphate system.[49,50] Hydronium substitution for various monovalent cations in autunite-type uranyl compounds has also been

https://doi.org/10.1021/acs.est.2c06648
Environ. Sci. Technol. 2023, 57, 255−265

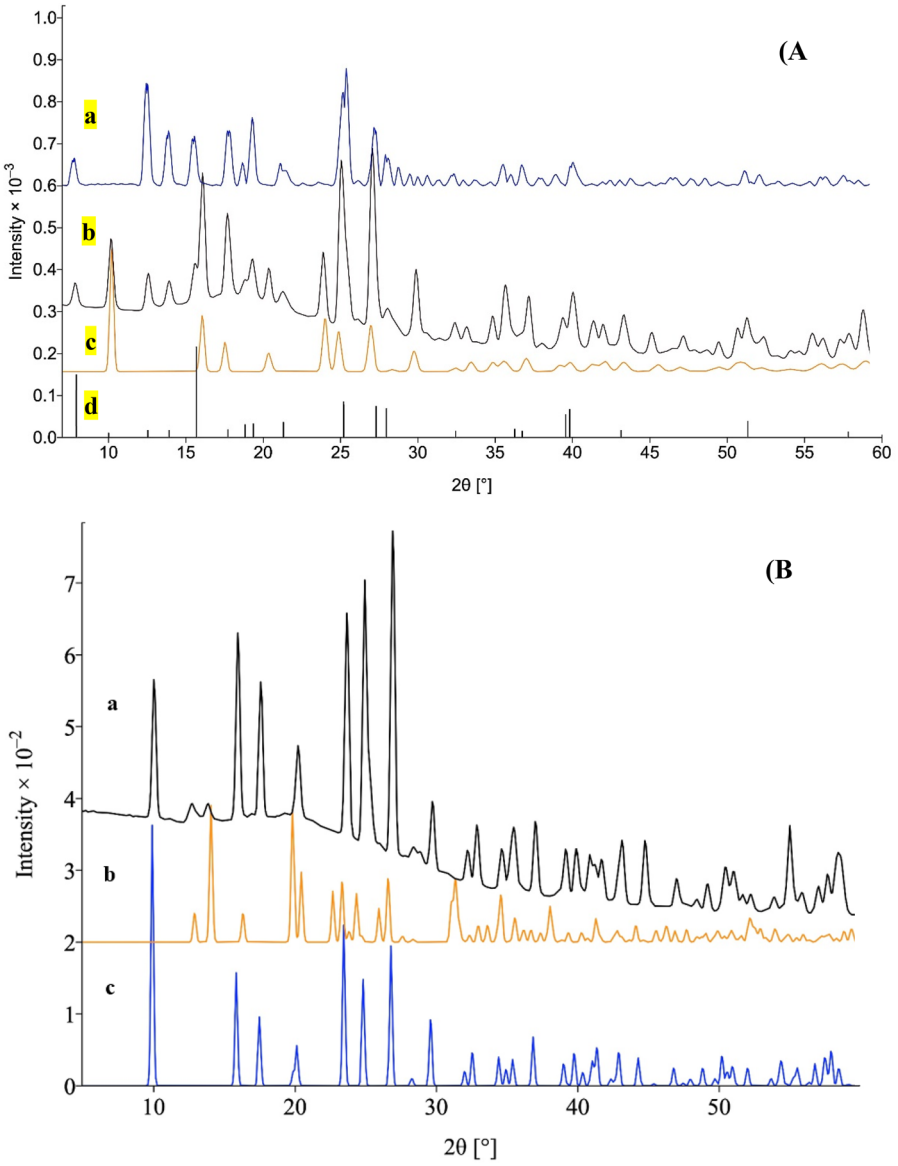

Figure 2. (A) Powder X-ray diffraction patterns of synthetic $Na[(UO_2)(AsO_4)](H_2O)_3$ reacted material from dissolution (a) and precipitation experiments (b) pH 3, compared to sodium uranyl arsenate (c) and trögerite (d). (B) Powder X-ray diffraction patterns of KUAs reacted material (a) compared to $(UO_2)(H_2AsO_4)_2(H_2O)_{(s)}$ (b) and potassium uranyl arsenate (c).

documented.[51−53] Furthermore, a reported single-crystal structure determination for KUAs assigned the formula $K_{0.91}(H_3O)_{0.09}[(UO_2)(AsO_4)](H_2O)_3$,[34] similar to that derived in the current study.

Equilibrium Concentrations for Dissolution and Precipitation Experiments. The results for the NaUAs and KUAs dissolution and precipitation experiments conducted in this study confirmed that equilibrium was reached within 2 d (Figure 1 and Figures S4 and S5), well under the 31 d duration of the experiments. The equilibrium concentrations (Table S2) of U and As obtained for all dissolution experiments with NaUAs and KUAs at pH 2 are close to equimolar (Figure 1a and e).

For experiments at pH 2, the molar ratios of U:As:Na of 1:1:0.72 were measured after the dissolution of NaUAs in aqueous solutions (Figure 1a and Figure S4a). In contrast, in precipitation experiments, the molar ratios of U:As:Na were 1:1:1.15 in solutions (Figure 1b and Figure S4b). Both results indicate that NaUAs do not have the end-member formula with a Na:U molar ratio of 1, but rather when the Na:U molar ratio is less than 1 because the interlayer of NaUAs also contains hydronium.

Upon dissolution of KUAs in aqueous solutions at pH 2, the molar ratios at equilibrium of U:As:K were 1:0.97:0.99 (Figure 1e and Figure S5a). However, precipitation reactions yielded an elevated K concentration in aqueous solution relative to U and As (Figure 1f and Figure S5b). Powder X-ray diffraction analyses of the recovered solids in this case revealed the presence of $(UO_2)(H_2AsO_4)_2(H_2O)_{(s)}$ (Figure 2B). This observation suggests that the secondary phase of $(UO_2)(H_2AsO_4)_2(H_2O)_{(s)}$ could have caused lower concentrations of U and As compared to K in the precipitation experiments with KUAs. Additionally, this phase could have influenced the chemical equilibrium and kinetics of the reactions affecting KUAs solubility. More research is needed to better understand the influence of secondary phases on soluble U and As concentrations in solution at acidic pH.

https://doi.org/10.1021/acs.est.2c06648
Environ. Sci. Technol. 2023, 57, 255−265

Table 2. Thermochemical cycles for calculation of ($\Delta H_{f\text{-}ox}$)) and ($\Delta H_{f\text{-}el}$) for NaUAs and KUAs[18,64−68]

Reaction	ΔH	KUAs ΔH (kJ/mol)	NaUAs ΔH (kJ/mol)
$Na_{0.5}(H_3O)_{0.5}[(UO_2)(AsO_4)]\cdot 2.5H_2O_{(s,\ 298\ K)} = 0.25Na_2O_{(soln,\ 976\ K)} + UO_{3(soln,\ 976\ K)} + 0.5As_2O_{5(soln,\ 976\ K)} + 3.25H_2O_{(g,\ 976\ K)}$	$\Delta H_1 = \Delta H_{ds}$		523.1 ± 21.7
$K_{0.9}(H_3O)_{0.1}[(UO_2)(AsO_4)]\cdot 2.5H_2O_{(xl,\ 298\ K)} = 0.45K_2O_{(soln,\ 976\ K)} + UO_{3(soln,\ 976\ K)} + 0.5As_2O_{5(soln,\ 976\ K)} + 2.65H_2O_{(g,\ 976\ K)}$	$\Delta H_1 = \Delta H_{ds}$	523.9 ± 27.8	
$As_2O_{5(xl,\ 298\ K)} = As_2O_{5(soln,\ 976\ K)}$	$\Delta H_2 = \Delta H_{ds}$	76.7 ± 0.8	76.7 ± 0.8
$UO_{3(xl,\ 298\ K)} = UO_{3(soln,\ 298\ K)}$	$\Delta H_3 = \Delta H_{ds}$	9.49 ± 1.53	9.49 ± 1.53
$Na_2O_{(s,\ 298\ K)} = Na_2O_{(soln,\ 976\ K)}$	$\Delta H_4 = \Delta H_{ds}$		−217.56 ± 4.25
$K_2O_{(s,\ 298\ K)} = K_2O_{(soln,\ 976\ K)}$	$\Delta H_4 = \Delta H_{ds}$	−318.0 ± 3.1	
$H_2O_{(l,\ 298\ K)} = H_2O_{(g,\ 976\ K)}$	$\Delta H_5 = \Delta H_{ds}$	69	69
$0.25Na_2O_{(xl,\ 298\ K)} + UO_{3(s,\ 298\ K)} + 3.25H_2O_{(g,\ 298\ K)} + 0.5As_2O_{5(s,\ 298\ K)} = Na_{0.5}(H_3O)_{0.5}[(UO_2)(AsO_4)]\cdot 2.5H_2O_{(xl,\ 298\ K)}$	$\Delta H_6 = \Delta H_{f\text{-}ox} = -\Delta H_1 + 0.5\Delta H_2 + \Delta H_3 + 0.25\Delta H_4 + 3.25\Delta H_5$		−305.4 ± 22.0
$0.45K_2O_{(xl,\ 298\ K)} + UO_{3(xl,\ 298\ K)} + 2.65\ H_2O_{(g,\ 298\ K)} + 0.5As_2O_5 = K_{0.9}(H_3O)_{0.1}[(UO_2)(AsO_4)]\cdot 2.5(H_2O)_{(xl,\ 298\ K)}$	$\Delta H_6 = \Delta H_{f\text{-}ox} = -\Delta H_1 + 0.5\Delta H_2 + \Delta H_3 + 0.45\Delta H_4 + 2.65\Delta H_5$	−436.4 ± 28.0	
$2As_{(s,\ 298\ K)} + 2.5O_{2(g,\ 298\ K)} = As_2O_{5(s,\ 298\ K)}$	$\Delta H_7 = \Delta H_f$	−926	−926
$U_{(xl,\ 298\ K)} + 1.5O_{2(g,\ 298\ K)} = UO_{3(xl,\ 298\ K)}$	$\Delta H_8 = \Delta H_f$	−1223.8 ± 0.8	−1223.8 ± 0.8
$2Na_{(s,\ 298\ K)} + 0.5O_{2(g,\ 298\ K)} = Na_2O_{(s,\ 298\ K)}$	$\Delta H_9 = \Delta H_f$		−414.8 ± 0.3
$2K_{(s,\ 298\ K)} + 0.5O_{2(g,\ 298\ K)} = K_2O_{(s,\ 298\ K)}$	$\Delta H_9 = \Delta H_f$	−363.2 ± 2.1	
$H_{2(g,\ 298\ K)} + 0.5O_{2(g,\ 298\ K)} = H_2O_{(g,\ 298\ K)}$	$\Delta H_{10} = \Delta H_f$	−285.8 ± 0.1	−285.8 ± 0.1
$0.5Na_{(xl,\ 298\ K)} + U_{(s,\ 298\ K)} + As_{(g,\ 298\ K)} + 4.5O_{2(g,\ 298\ K)} + 2.5H_{2(g,\ 298\ K)} = Na_{0.5}(H_3O)_{0.5}[(UO_2)(AsO_4)]\cdot 2.5H_2O_{(xl,\ 298\ K)}$	$\Delta H_{11} = \Delta H_{f\text{-}el} = \Delta H_6 + 0.5\Delta H_7 + \Delta H_8 + 0.25\Delta H_9 + 2.5\Delta H_{10}$		−3025 ± 22
$0.9K_{(xl,\ 298\ K)} + U_{(xl,\ 298\ K)} + As_{(xl,\ 298\ K)} + 4.3O_{2(g,\ 298\ K)} + 2.65H_{2(g,298\ K)} = K_{0.9}(H_3O)_{0.1}[(UO_2)(AsO_4)\cdot 2.5H_2O_{(xl,\ 298\ K)}$	$\Delta H_{11} = \Delta H_{f\text{-}el} = \Delta H_6 + 0.5\Delta H_7 + \Delta H_8 + 0.45\Delta H_9 + 2.65\Delta H_{10}$	−3000 ± 28	

For both NaUAs and KUAs dissolution experiments at pH 3, the concentrations of U and As in solution were up to 93% lower than observed in solutions at pH 2 (Figure 1a, c, e, and g and Figures S4a, c and S5a, c). The aqueous solutions in precipitation experiments at pH 3 contained from 65% to 97% less soluble U and As than experiments at pH 2 (Figure 1b, d, f, h and Figures S4b, d and S5b, d).

The changes in soluble U and As concentrations in solution as a function of pH could be affected by the formation of secondary phases. The secondary phase trögerite $(UO_2)_3(AsO_4)_2\cdot 12H_2O_{(s)}$[25,54] was present in the solids recovered from dissolution and precipitation experiments with NaUAs in solutions at pH 3. Thus, the soluble concentrations of U and As are not only controlled by the dissolution of NaUAs, but also by the secondary phase trögerite in these pH conditions [Figure 2A(a−d), Figure S6]. X-ray diffraction analysis of residual solids from dissolution and precipitation experiments in this pH confirmed that KUAs were the only phase present (Figure S7). The presence of $(UO_2)(H_2AsO_4)_2(H_2O)_{(s)}$ was not detected by p-XRD in these experiments. However, XRD is not a trace technique; therefore, the presence of this phase at a concentration below the detection of this instrument cannot be discarded.

Application of the species name trögerite is inconsistent in the literature. The International Mineralogical Association states its formula is $(H_3O)(UO_2)(AsO_4)\cdot 3H_2O$ and attributes this to a publication from 1871.[55] The same formula appears several times in the literature associated with the name trögerite over the years, and Locock and Burns listed trögerite with this formula along with autunite group minerals, implying that it has the autunite-type structure.[56] Chernorukov et al. referred to the compound $(UO_2)_3(AsO_4)_2\cdot 12H_2O$ as trögerite and argued that this composition likely corresponds to the natural mineral.[54] It is possible that the name trögerite has been applied to more than one mineral species in the literature. Herein, we equate trögerite with $(UO_2)_3(AsO_4)_2\cdot 12H_2O$ according to Chernorukov et al.[54] Although the crystal structure of this phase has not been determined, it is clearly not an autunite group mineral as the different U:As ratio mandates a different structural connectivity.

Solubility Product Measurements. The log K_{sp} obtained using the concentrations at equilibrium from the solubility experiments in speciation calculations using PFLOTRAN ranged from −23.50 to −22.96 for NaUAs and from −23.87 to −23.38 for KUAs. We based our calculations on the dissolution and precipitation experiments (Table 1 and Tables S6 and S7). The obtained log K_{sp} values for NaUAs and KUAs are within 1 order of magnitude and with a maximum difference of 3.4% between dissolution and precipitation experiments at pH 2 and 3. Thus, the log K_{sp} values for NaUAs and KUAs are independent of pH within experimental error by both dissolution and precipitation experiments (Table 1).

The solubility products obtained for NaUAs and KUAs at pH 2 were within 1 order of magnitude compared to those at pH 3 (Table 1). However, the soluble concentrations of U and As in dissolution and precipitation experiments at pH 3 were controlled by NaUAs and the secondary phase trögerite. We estimated a log K_{sp} for trögerite of −47.97 at dissolution and at pH 3, which is within 2 orders of magnitude of the value reported in a previous study of −45.93[25] (Table 1). The log K_{sp} obtained for NaUAs was not sensitive to the deficiency of Na in the stoichiometry of this solid. For example, we varied the stoichiometry of Na to estimate the log K_{sp} for NaUAs using the software PFLOTRAN with Na molarities of 0.25, 0.48, 0.7, and 1. The log K_{sp} values for varying Na stoichiometries were within 2.8% using the equilibrium concentrations in dissolution and precipitation experiments at pH 2 and 3, which is within expected experimental error (Table S6). The soluble concentrations of U and As in precipitation experiments at pH 2 were controlled by KUAs and the secondary phase $(UO_2)(H_2AsO_4)_2(H_2O)_{(s)}$. We also estimated a log K_{sp} for $(UO_2)(H_2AsO_4)_2(H_2O)_{(s)}$ of −46.97 (Table 1) for precipitation at pH 2 which is within 1 order of magnitude of the log K_{sp} from trögerite reported in a previous study.[25]

https://doi.org/10.1021/acs.est.2c06648
Environ. Sci. Technol. 2023, 57, 255−265

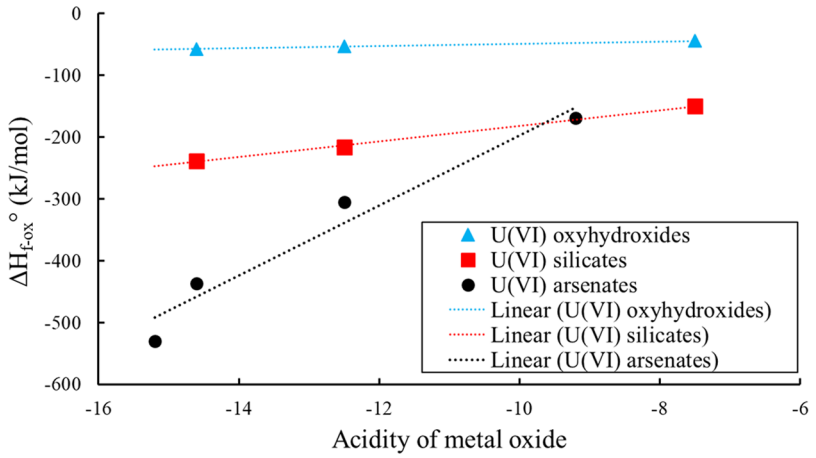

Figure 3. Plot of the standard enthalpy of formation from the oxides ($\Delta H_{f\text{-}ox}$) for uranyl oxyhydroxides, silicates, and arsenates versus the acidity of the alkali metal oxide. Data for the U(VI) oxyhydroxide and silicates taken from Shvareva et al.[45] Linear regression fits: U(VI) oxyhydroxide $y = 1.868x - 30.491$; $R^2 = 0.998$; U(VI) silicates $y = 12.595x - 56.208$; $R^2 = 0.998$; U(VI) arsenate $y = 56.645x + 369.02$; $R^2 = 0.955$.

The log K_{sp} obtained using thermodynamic modeling was not sensitive to the considerations of uranyl arsenate complexes obtained by Rutsch et al.[25] The log K_{sp} values calculated with and without uranyl arsenate aqueous complexes were 2.66% for NaUAs and KUAs for the dissolution experiments at pH 2 and 3 (Table 1, Tables S6−S8). The uranyl arsenate complexes predominant at acidic pH are $UO_2(H_2AsO_4)(H_2O)^{3+}$, $(UO_2)_3(AsO_4)_2{\cdot}4H_2O$, $(UO_2)_3(AsO_4)_2{\cdot}12H_2O$, $UO_2H_2AsO_4^+$, $UO_2(HAsO_4)$, and $UO_2(H_2AsO_4)_2$.[25,31,57] We considered all of these uranyl arsenate complexes in the PFLOTRAN simulations to estimate the log K_{sp} values reported in this study (Table 1 and Tables S6 and S7). All the main input species considered for the PFLOTRAN simulations conducted in this study are reported in Table S4. The log K_{sp} values obtained without considering the aqueous uranyl arsenate complexes in the PFLOTRAN simulations are reported in Table S8. Our log K_{sp} values are within the range of those reported in previous studies in which the log K_{sp} for $NaAsUO_6{\cdot}3H_2O$ ranged from −21.86 to −23.5 and for $KAsUO_6{\cdot}3H_2O$ ranged from −22.65 to −24.00.[26,28,58,59] One of these studies considered aqueous uranyl arsenate complexes for determining log K_{sp} values.[28] However, other studies did not consider aqueous uranyl complexes in the determination of the log K_{sp} values.[26,58,59] More research is needed to determine the relevance of uranyl arsenate complexes in U and As aqueous speciation after dissolution of uranyl arsenate solids.

Standard-State Enthalpy (ΔH_f), Gibbs Free Energy (ΔG_f), and Entropy of formation (ΔS_f). The measured enthalpies of drop solution for each compound can be found in Table S9, and the relevant calorimetric cycles for NaUAs and KUAs are in Table 2. The calculated standard enthalpies of formation from the oxides ($\Delta H_{f\text{-}ox}$) are −305.4 ± 22.0 and −436.4 ± 28.0 kJ mol^{-1} for NaUAs and KUAs, respectively. Calculated $\Delta H_{f\text{-}el}$ values are −3025 ± 22 and −3000 ± 28 kJ mol^{-1} for NaUAs and KUAs, respectively.

Dzik et al.[18] provided high-temperature calorimetric measurements for a series of uranyl arsenate phases with alkali, alkali-earth, and transition metal cations present in the interlayer. Their study suggested an overall stoichiometry for the KUAs phase of $K_{0.87}[(UO_2)(AsO_4)_{1.05}]{\cdot}3H_2O$ with $\Delta H_{f\text{-}ox}$ and $\Delta H_{f\text{-}el}$ values of −363.7 ± 14.1 and −3089 ± 14 kJ mol^{-1}, respectively.[18] We note that in their study they assumed an overall formula $K[(UO_2)(AsO_4)_{1.05}]{\cdot}3H_2O$, and did not include additional hydronium to charge balance the structure. The previous work from Dzik et al., evaluated the relationship between the $\Delta H_{f\text{-}ox}$ and the acidity of the cation present (derived from the acidity value of the metal oxide) and found it to be linear ($R^2 = 0.8571$).[18] With the data presented herein, we observe a similar relationship between the $\Delta H_{f\text{-}ox}$ and the acidity and an improved fit once additional hydronium is included ($R^2 = 0.9549$) (Figure S8). These data indicate that as the metal cation becomes more acidic, the enthalpy of formation for the uranyl arsenates becomes less exothermic. This relationship between the metal cation acidity and the enthalpy of formation has also been reported[45] for uranyl oxyhydroxide and uranyl silicate phases (Figure 3). The slopes for uranyl arsenates were steeper compared to the silicate and oxyhydroxide phases (Figure 3), suggesting a larger interaction between the uranyl arsenate sheet and the interstitial cations compared to that of the silicate and oxyhydroxide phases.

The calculated values of ΔG_f for KUAs are at least 100 kJ mol^{-1} more negative than those obtained for NaUAs, indicating that the KUAs is more thermodynamically stable than NaUAs. The calculated values for ΔG_f NaUAs are −2456.8 kJ mol^{-1} at pH 2 and −2455 kJ mol^{-1} for pH 3. The calculated values for ΔG_f KUAs are −2582 kJ mol^{-1} for pH 2 and −2581 kJ mol^{-1} for pH 3 (Table 3). The calculated values of ΔS_f for NaUAs are at least 500 J mol^{-1} K^{-1} more negative than those obtained for KUAs. The ΔS_f values for NaUAs are −1907 J mol^{-1} K^{-1} at pH 2 and −1913 J mol^{-1} K^{-1} for pH 3. The calculated values of ΔS_f for KUAs are −1401 J mol^{-1} K^{-1} for pH 2 and −1407 J mol^{-1} K^{-1} for pH 3 (Table 3). Our results are similar to those found in a previous study for uranyl hydrogen phosphate.[27]

Table 3. Calculated Gibbs Free Energy (ΔG_f) and Entropy (ΔS_f) for NaUAs and KUAs

Experimental pH	Solid phase	ΔG_f	ΔS_f
2	NaUAs	−2455	−1907
3	NaUAs	−2455	−1913
2	KUAs	−2582	−1401
3	KUAs	−2581	−1407

https://doi.org/10.1021/acs.est.2c06648
Environ. Sci. Technol. 2023, 57, 255−265

Insights about Solubility of Uranyl Arsenate Solids. The solubility product constants obtained at pH 2 and 3 in this study for KUAs and NaUAs are within 1 order of magnitude, which is within expected experimental error for soluble measured concentrations. The substitution of cations are known to impact the number of H_2O molecules in the interlayer of UAs.[26] Uranium and As form anionic two-dimensional layers of the type $[P(As)UO_6]^{n-}{}_{2\infty}$ known by an increased stability.[26] For instance, the role of hydronium in the UAs structure needs to be further understood.

The occurrence of hydronium $(H_3O)^+$ in the interlayer region of compounds containing uranyl phosphate and arsenate sheets with the autunite topology is lacking an understanding of the details of the substitution of hydronium for other monovalent cations in the interlayers of autunite-structure compounds. In the case of autunite-structure compounds, the importance of hydronium is well established. The structure of the hydronium end-member compound $(H_3O)[(UO_2)(PO_4)](H_2O)_3$ was reported by Morosin and is a hydrogen ion solid electrolyte.[60] The structure of (H_3O)-$[(UO_2)(AsO_4)](H_2O)_3$ was determined more recently, including the location of the H atoms corresponding to the hydronium ions.[61] Earlier determinations of the structures of autunite compounds containing monovalent cations also noted the presence of hydronium.[34] However, we are missing more information about the substitution of hydronium for monovalent cations in the interlayers of autunite-structure compounds, as hydronium is rare in mineral structures, and it is challenging to identify it.

The presence of hydronium is difficult to directly demonstrate by spectroscopy, and in the case of chemically well-characterized materials, its presence can be demonstrated by the electroneutrality principle. Locally, in the interlayer region, hydronium could substitute for a H_2O group or a monovalent cation, or the H atom may be largely mobile, which is consistent with the compound $(H_3O)[(UO_2)(PO_4)]$-$(H_2O)_3$ that exhibits rapid H^+ ion conductivity.[62] In the current case, the hydronium ion content was determined by establishing the composition of the compounds by chemical analyses, with hydronium assumed for charge balance.

The identification of trögerite in the residual solids may relate to the role of H_3O^+ which is present with Na in the interlayer region of the structure of NaUAs used in the dissolution experiments; trögerite was also identified in precipitation experiments with NaUAs at pH 3. Formation of trögerite in this study caused a decrease in the final soluble U and As concentrations in solution and with a resulting final solution pH in the range of 3. The formation of this secondary mineral is consistent with findings reported in other studies.[28,54]

The aqueous speciation of U, As, Na, and K influences the dissolution and precipitation reactions for the determination of the log K_{sp} values of NaUAs and KUAs solids. For example, the formation of uranyl arsenate complexes has been reported in the literature and cannot be ignored in the determination of the solubility constants. According to the literature, at pH 2 and 3, U(VI) will be present as UO_2^{2+}, while As(V) could be present as 50% to 75% of H_3AsO_4 and $H_2AsO_4^{1-}$, and Na could be a free ion Na^{1+}.[63] However, we considered other aqueous complexes in the dissolution reactions with the PFLOTRAN modeling such as $UO_2H_2AsO_4{}^+{}_{(aq)}$, $UO_2HAsO_{4(aq)}$, and $UO_2(H_2AsO_4)_2$.,[31,57] The log K_{sp} was not sensitive to these aqueous uranyl complexes as they differed only between 2.06% and 2.43%. Future research is necessary to determine how aqueous uranyl arsenate complexes influence aqueous speciation of U and As as a function of pH.

Environmental Implications. The solubility and thermodynamic data obtained for NaUAs and KUAs in this study contribute new information that will underpin predictions of U and As dissolutions using chemical equilibrium and reactive transport models. The thermodynamic variables obtained can be used in reactive transport models to interpret and predict the solubilities of U and As. The findings from this study can be useful for risk assessment and risk reduction studies where anthropogenic activities such as mining and nuclear weapons development have resulted in contamination.

■ ASSOCIATED CONTENT

Supporting Information

The Supporting Information is available free of charge at https://pubs.acs.org/doi/10.1021/acs.est.2c06648.

Additional materials and methods, nine tables, and eight figures (PDF)

■ AUTHOR INFORMATION

Corresponding Author

José M. Cerrato − *Department of Civil, Construction & Environmental Engineering, MSC01 1070, University of New Mexico, Albuquerque, New Mexico 87131, United States; Center for Water and the Environment, UNM, Albuquerque, New Mexico 87131, United States;* orcid.org/0000-0002-2473-6376; Phone: (1) (505) 277-2722; Email: jcerrato@unm.edu; Fax: (1) (505) 277-1918

Authors

Isabel Meza − *Department of Civil, Construction & Environmental Engineering, MSC01 1070, University of New Mexico, Albuquerque, New Mexico 87131, United States; Center for Water and the Environment, UNM, Albuquerque, New Mexico 87131, United States*

Jorge Gonzalez-Estrella − *School of Civil and Environmental Engineering, College of Engineering, Architecture, and Technology, Oklahoma State University, Stillwater, Oklahoma 74078, United States;* orcid.org/0000-0002-4873-0454

Peter C. Burns − *Department of Civil and Environmental Engineering and Earth Sciences and Department of Chemistry and Biochemistry, University of Notre Dame, Notre Dame, Indiana 46556, United States;* orcid.org/0000-0002-2319-9628

Virginia Rodriguez − *Department of Civil and Environmental Engineering and Earth Sciences and Department of Chemistry and Biochemistry, University of Notre Dame, Notre Dame, Indiana 46556, United States;* orcid.org/0000-0002-8728-4004

Carmen A. Velasco − *Department of Civil, Construction & Environmental Engineering, MSC01 1070, University of New Mexico, Albuquerque, New Mexico 87131, United States; Center for Water and the Environment, UNM, Albuquerque, New Mexico 87131, United States*

Ginger E. Sigmon − *Department of Civil and Environmental Engineering and Earth Sciences and Department of Chemistry and Biochemistry, University of Notre Dame, Notre Dame, Indiana 46556, United States*

https://doi.org/10.1021/acs.est.2c06648
Environ. Sci. Technol. 2023, 57, 255−265

Jennifer E. S. Szymanowski − *Department of Civil and Environmental Engineering and Earth Sciences and Department of Chemistry and Biochemistry, University of Notre Dame, Notre Dame, Indiana 46556, United States*
Tori Z. Forbes − *Department of Chemistry, University of Iowa, Iowa City, Iowa 52242, United States;* orcid.org/0000-0002-5234-8127
Lindsey M. Applegate − *Department of Chemistry, University of Iowa, Iowa City, Iowa 52242, United States*
Abdul-Mehdi S. Ali − *Department of Earth and Planetary Sciences, MSC03 2040, University of New Mexico, Albuquerque, New Mexico 87131, United States*
Peter Lichtner − *Center for Water and the Environment, UNM, Albuquerque, New Mexico 87131, United States*

Complete contact information is available at: https://pubs.acs.org/10.1021/acs.est.2c06648

Notes

The authors declare no competing financial interest.

■ ACKNOWLEDGMENTS

Funding for this research was provided by the National Science Foundation (CAREER Award 1652619, CREST Award 1914490) and the National Institute of Environmental Health Sciences (Superfund Research Program Awards 1 P42 ES025589 and R01ES027145). P.C.B.'s contribution to this work was funded by the Chemical Sciences, Geosciences and Biosciences Division, Office of Basic Energy Sciences, Office of Science, U.S. Department of Energy, Grant No. DE-FG02-07ER15880. Partial funding for the PerkinElmer NexION ICP/MS coupled with the ESI SeaFast SP3 was provided by the UNM Office of the Vice President for Research (OVPR) and the College of Art and Sciences. We also would like to acknowledge PerkinElmer and ESI for their valuable technical and applications support for the use of their analytical instruments used to support this research project and providing quality data. Any opinions, findings, and conclusions or recommendations expressed in this publication are those of the author(s) and do not necessarily reflect the views of the National Science Foundation, the National Institutes of Health, or the U.S. Department of Energy. The TOC art was created with www.BioRender.com.

■ REFERENCES

(1) Coyte, R. M.; Vengosh, A. Factors controlling the risks of co-occurrence of the redox-sensitive elements of arsenic, chromium, vanadium, and uranium in groundwater from the eastern United States. *Environ. Sci. Technol.* **2020**, *54* (7), 4367−4375.
(2) Das, N.; Das, A.; Sarma, K. P.; Kumar, M. Provenance, prevalence and health perspective of co-occurrences of arsenic, fluoride and uranium in the aquifers of the Brahmaputra River floodplain. *Chemosphere* **2018**, *194*, 755−772.
(3) Yadav, S. K.; Ramanathan, A. L.; Kumar, M.; Chidambaram, S.; Gautam, Y. P.; Tiwari, C. Assessment of arsenic and uranium co-occurrences in groundwater of central Gangetic Plain, Uttar Pradesh, India. *Environ. Earth Sci.* **2020**, *79* (6), 154.
(4) Sobel, M.; Sanchez, T. R.; Zacher, T.; Mailloux, B.; Powers, M.; Yracheta, J.; Harvey, D.; Best, L. G.; Bear, A. B.; Hasan, K.; Thomas, E.; Morgan, C.; Aurand, D.; Ristau, S.; Olmedo, P.; Chen, R.; Rule, A.; O'Leary, M.; Navas-Acien, A.; George, C. M.; Bostick, B. Spatial relationship between well water arsenic and uranium in Northern Plains native lands. *Environ. Pollut.* **2021**, *287*, 117655.
(5) Corkhill, C. L.; Crean, D. E.; Bailey, D. J.; Makepeace, C.; Stennett, M. C.; Tappero, R.; Grolimund, D.; Hyatt, N. C. Multi-scale investigation of uranium attenuation by arsenic at an abandoned uranium mine, South Terras. *NPJ. Mater. Degrad.* **2017**, *1* (1), 19.
(6) Hoover, J.; Gonzales, M.; Shuey, C.; Barney, Y.; Lewis, J. Elevated arsenic and uranium concentrations in unregulated water sources on the Navajo Nation, USA. *Expos. Health.* **2017**, *9* (2), 113−124.
(7) Hoover, J. H.; Coker, E.; Barney, Y.; Shuey, C.; Lewis, J. Spatial clustering of metal and metalloid mixtures in unregulated water sources on the Navajo Nation - Arizona, New Mexico, and Utah, USA. *Sci. Total Environ.* **2018**, *633*, 1667−1678.
(8) *Toxicological Profile for Arsenic*; Agency for Toxic Substances and Disease Registry, U.S. Department of Health: Atlanta, GA, 2000.
(9) Keith, S.; Faroon, O.; Roney, N.; Scinicariello, F.; Wilbur, S.; Ingerman, L.; Llados, F.; Plewak, D.; Wohlers, D.; Diamond, G.*Toxicological Profile for Uranium*Agency for Toxic Substances and Disease Registry, U.S. Department of Health: Atlanta, GA, 2013.
(10) Donahue, R.; Hendry, M. J. Geochemistry of arsenic in uranium mine mill tailings, Saskatchewan, Canada. *Appl. Geoch.* **2003**, *18* (11), 1733−1750.
(11) Blake, J. M.; Avasarala, S.; Artyushkova, K.; Ali, A.-M. S.; Brearley, A. J.; Shuey, C.; Robinson, W. P.; Nez, C.; Bill, S.; Lewis, J.; Hirani, C.; Pacheco, J. S. L.; Cerrato, J. M. Elevated Concentrations of U and Co-occurring Metals in Abandoned Mine Wastes in a Northeastern Arizona Native American Community. *Environ. Sci. Technol.* **2015**, *49* (14), 8506−8514.
(12) Blake, J. M.; De Vore, C. L.; Avasarala, S.; Ali, A.-M.; Roldan, C.; Bowers, F.; Spilde, M. N.; Artyushkova, K.; Kirk, M. F.; Peterson, E.; Rodriguez-Freire, L.; Cerrato, J. M. Uranium mobility and accumulation along the Rio Paguate, Jackpile Mine in Laguna Pueblo, NM. *Environ. Sci. Process. Impacts* **2017**, *19* (4), 605−621.
(13) Larson, L. N.; Kipp, G. G.; Mott, H. V.; Stone, J. J. Sediment pore-water interactions associated with arsenic and uranium transport from the North Cave Hills mining region, South Dakota, USA. *Appl. Geoch.* **2012**, *27* (4), 879−891.
(14) Blake, J. M.; Avasarala, S.; Ali, A.-M. S.; Spilde, M.; Lezama-Pacheco, J. S.; Latta, D.; Artyushkova, K.; Ilgen, A. G.; Shuey, C.; Nez, C.; Cerrato, J. M. Reactivity of As and U co-occurring in Mine Wastes in northeastern Arizona. *Chem. Geol.* **2019**, *522*, 26−37.
(15) Mittal, A. K.Abandoned mines: information on the number of hardrock mines, cost of clean up, and value of financial assurances (testimony before the subcommittee on energy and mineral resources, Committee on Natural Resources, House of Representatives No. GAO-11-834T), 2011. United States Accountability Office. https://www.gao.gov/assets/gao-11-834t.pdf (accessed November 29, 2022).
(16) Dzik, E. A.; Lobeck, H. L.; Zhang, L.; Burns, P. C. Thermodynamic properties of phosphate members of the meta-autunite group: A high-temperature calorimetric study. *J. Chem. Thermodyn.* **2017**, *114*, 165−171.
(17) Finch, R. M. T.*Systematics and Paragenesis of Uranium Minerals.*; Argonne National Laboratory, Mineralogical Institute, University of Japan, 1999; Vol. *1*, p 87.
(18) Dzik, E. A.; Lobeck, H. L.; Zhang, L.; Burns, P. C. High-temperature calorimetric measurements of thermodynamic properties of uranyl arsenates of the meta-autunite group. *Chem. Geol.* **2018**, *493*, 353−358.
(19) Miyawaki, R.Commission on new minerals, nomenclature and classification. http://cnmnc.main.jp/ (accessed September 11, 2022).
(20) Frost, R. L.; Carmody, O.; Erickson, K. L.; Weier, M. L. Near-infrared spectroscopy to uranyl arsenates of the autunite and metaautunite group. *pectrochim. Acta A Mol. Biomol. Spectrosc.* **2005**, *61* (8), 1923−1927.
(21) Burns, P. C.; Sigmon, G. E.*Uranium: Cradle to Grave*; Mineralogical Association of Canada: Winnipeg, 2013; Vol. *43*.
(22) Spano, T. L.; Dzik, E. A.; Sharifironizi, M.; Dustin, M. K.; Turner, M.; Burns, P. C. Thermodynamic investigation of uranyl vanadate minerals: Implications for structural stability. *Am. Mineral.* **2017**, *102* (6), 1149−1153.
(23) Troyer, L. D.; Tang, Y.; Borch, T. Simultaneous reduction of arsenic(V) and uranium(VI) by mackinawite: role of uranyl arsenate

precipitate formation. *Environ. Sci. Technol.* **2014**, *48* (24), 14326−14334.
(24) Liu, H.-K.; Ramachandran, E.; Chen, Y.-H.; Chang, W.-J.; Lii, K.-H. High-temperature, high-pressure hydrothermal synthesis, characterization, and structural relationships of layered uranyl arsenates. *Inorg. Chem.* **2014**, *53* (17), 9065−9072.
(25) Nipruk, O. V.; Chernorukov, N. G.; Pykhova, Y. P.; Godovanova, N. S.; Eremina, A. A. State of uranyl phosphates and arsenates in aqueous solutions. *Radiochemistry* **2011**, *53* (5), 483.
(26) Chernorukov, N. G.; Karyakin, N. V. The physical chemistry of the compounds MIP(As)UO_6 (MI = H, Li, Na, K, Rb, Cs) and their crystalline hydrates. *Russ. Chem. Rev.* **1995**, *64* (10), 913−927.
(27) Gorman-Lewis, D.; Shvareva, T.; Kubatko, K.-A.; Burns, P. C.; Wellman, D. M.; McNamara, B.; Szymanowski, J. E. S.; Navrotsky, A.; Fein, J. B. Thermodynamic properties of autunite, uranyl hydrogen phosphate, and uranyl orthophosphate from solubility and calorimetric measurements. *Environ. Sci. Technol.* **2009**, *43* (19), 7416−7422.
(28) Nipruk, O. V.; Chernorukov, N. G.; Elipasheva, E. V.; Klinshova, K. A.; Bakhmetev, M. O. State of uranyl arsenates $M^IAsUO_6{\cdot}nH_2O$ (M^I-H^+, Li^+, Na^+, K^+, Rb^+, Cs^+, NH_4^+) in aqueous solution. *J. Radioanal. Nucl. Chem.* **2020**, *324* (1), 233−244.
(29) Gorman-Lewis, D.; Fein, J. B.; Burns, P. C.; Szymanowski, J. E.; Converse, J. Solubility measurements of the uranyl oxide hydrate phases metaschoepite, compreignacite, Na-compreignacite, becquerelite, and clarkeite. *J. Chem. Thermodyn.* **2008**, *40* (6), 980−990.
(30) Gorman-Lewis, D.; Burns, P. C.; Fein, J. B. Review of uranyl mineral solubility measurements. *J. Chem. Thermodyn.* **2008**, *40* (3), 335−352.
(31) Rutsch, M.; Geipel, G.; Brendler, V.; Bernhard, G.; Nitsche, H. Interaction of uranium(VI) with arsenate(V) in aqueous solution studied by time-resolved laser-induced fluorescence spectroscopy (TRLFS). *Radiochim. Acta* **1999**, *86*, 135−141.
(32) Gezahegne, W. A.; Hennig, C.; Tsushima, S.; Planer-Friedrich, B.; Scheinost, A. C.; Merkel, B. J. EXAFS and DFT investigations of uranyl arsenate complexes in aqueous solution. *Environ. Sci. Technol.* **2012**, *46* (4), 2228−2233.
(33) Gonzalez-Estrella, J.; Meza, I.; Burns, A. J.; Ali, A.-M. S.; Lezama-Pacheco, J. S.; Lichtner, P.; Shaikh, N.; Fendorf, S.; Cerrato, J. M. Effect of bicarbonate, calcium, and pH on the reactivity of As(V) and U(VI) mixtures. *Environ. Sci. Technol.* **2020**, *54*, 3979−3987.
(34) Locock, A. J.; Burns, P. C.; Duke, M. J. M.; Flynn, T. M. Monovalent cations in structures of the meta-autunite group. *Can. Mineral.* **2004**, *42* (4), 973−996.
(35) Suleimanov, E. V.; Chernorukov, N. G.; Veridusova, V. V. Physical chemistry of magnesium and calcium uranophosphate and uranoarsenate $A^{II}(B^{V}UO_6)_2{\cdot}nH_2O$. *Radiochemistry* **2006**, *48* (2), 159−161.
(36) Lichtner, P. C.; Hammond, G. E.; Lu, C.; Karra, S.; Bisht, G.; Andre, B.; Mills, R. T.; Kumar, J.; Frederick, J. M.*PFLOTRAN User Manual*, 2019.
(37) ThermoChimie Thermodynamic Database, 2019. https://www.thermochimie-tdb.com/ (accessed August 31, 2022).
(38) Dong, W.; Brooks, S. C. Determination of the formation constants of ternary complexes of uranyl and carbonate with alkaline earth metals (Mg^{2+}, Ca^{2+}, Sr^{2+}, and Ba^{2+}) using anion exchange method. *Environ. Sci. Technol.* **2006**, *40* (15), 4689−4695.
(39) Dong, W.; Brooks, S. C. Formation of Aqueous $MgUO_2(CO_3)_3^{2-}$ Complex and Uranium Anion Exchange Mechanism onto an Exchange Resin. *Environ. Sci. Technol.* **2008**, *42* (6), 1979−1983.
(40) Guillaumont, R. G.; Fanghänel, T.; Fuger, J.; Ingmar, G.; Volker, N.; Palmer, D. A.; Rand, M. H.*Update on the Chemical Thermodynamics of Uranium, Plutonium, Americium, and Technetium*; Organization for Economic Co-Operation and Development: Paris, 2004.
(41) Giffaut, E.; Grivé, M.; Blanc, P.; Vieillard, P.; Colàs, E.; Gailhanou, H.; Gaboreau, S.; Marty, N.; Madé, B.; Duro, L. Andra thermodynamic database for performance assessment: ThermoChimie. *Appl. Geochem.* **2014**, *49*, 225−236.
(42) Navrotsky, A. Progress and New Directions in High-Temperature Calorimetry. *Phys. Chem. Miner.* **1977**, *2* (1−2), 89.
(43) Navrotsky, A. Progress and new directions in high temperature calorimetry revisited. *Phys. Chem. Miner.* **1997**, *24* (3), 222.
(44) Navrotsky, A. Progress and new directions in calorimetry: a 2014 perspective. *J. Am. Ceram. Soc.* **2014**, *97* (11), 3349−3359.
(45) Shvareva, T. Y.; Fein, J. B.; Navrotsky, A. Thermodynamic properties of uranyl minerals: constraints from calorimetry and solubility measurements. *Ind. Eng. Chem. Res.* **2012**, *51* (2), 607−613.
(46) Cox, J. D.; Wagman, D. D.; Medvedev, V. A.*CODATA Key Values for Thermodynamics*; Hemisphere Publishing Corp., 1989.
(47) Nordstrom, D. K.; Archer, D. G.Arsenic thermodynamic data and environmental geochemistry. In *Arsenic in Ground Water*; Welch, A. H.; Stollenwerk, K. G., Eds.; Kluwer Academic Publishing: Boston, 2003; pp 1−25.
(48) Mills, S. J.; Birch, W. D.; Kolitsch, U.; Mumme, W. G.; Grey, I. E. Lakebogaite, $CaNaFe_2^{3+}H(UO_2)_2(PO_4)_4(OH)_2(H_2O)_8$, a new uranyl phosphate with a unique crystal structure from Victoria, Australia. *Am. Mineral.* **2008**, *93* (4), 691−697.
(49) Ondrus, P.; Veselovsky, F.; Skala, R.; Cisarova, I.; Hlousek, J.; Fryda, J.; Vavrin, I.; Cejka, J.; Gabasova, A. New naturally occurring phases of secondary origin from Jachymov (Joachimsthal). *J. Czech Geol. Soc.* **1997**, *42* (4), 77−108.
(50) Clavier, N.; Crétaz, F.; Szenknect, S.; Mesbah, A.; Poinssot, C.; Descostes, M.; Dacheux, N. Vibrational spectroscopy of synthetic analogues of ankoleite, chernikovite and intermediate solid solution. *Spectrochim. Acta B: At. Spectrosc.* **2016**, *156*, 143−150.
(51) Ross, M.; Evans Jr, H. Studies of the torbernite minerals (III): role of the interlayer oxonium, potassium, and ammonium ions, and water molecules. *Am. Mineral.* **1965**, *50* (1−2), 1−12.
(52) Ross, M.; Evans Jr, H.; Appleman, D. Studies of the torbernite minerals (II): The crystal structure of meta-torbernite. *Am. Mineral.* **1964**, *49* (11−12), 1603−1621.
(53) Ross, M.; Evans Jr, H. T. Studies of the torbernite minerals (i): the crystal structure of abernathyite and the structurally related compounds $NH_4(UO_2AsO_4){\cdot}3H_2O$ and $K(H_3O)(UO_2AsO_4)_2{\cdot}6H_2O$. *Am. Mineral.* **1964**, *49* (11−12), 1578−1602.
(54) Chernorukov, N.; Nipruk, O.; Knyazev, A.; Pykhova, Y. P. Synthesis and study of uranyl arsenate $(UO_2)_3(AsO_4)_2{\cdot}12H_2O$. *Russ. J. Inorg. Chem.* **2011**, *56* (2), 163−167.
(55) Weisbach, A. Vorläufige Mitteilung - Trögerit, Walpurgin. *Neues Jahrb. Mineral.* **1871**, 869−870.
(56) Locock, A. J.; Burns, P. C. Structures and syntheses of layered and framework amine-bearing uranyl phosphate and uranyl arsenates. *J. Solid State Chem.* **2004**, *177* (8), 2675−2684.
(57) He, M.; Liu, X.; Cheng, J.; Lu, X.; Zhang, C.; Wang, R. Uranyl arsenate complexes in aqueous solution: Insights from first-principles molecular dynamics simulations. *Inorg. Chem.* **2018**, *57* (10), 5801−5809.
(58) Chukhlantsev, V. G.; Sharova, A. K. Solubility products of uranyl arsenates. *Russ. J. Inorg. Chem.* **1956**, *1* (1), 39−44.
(59) Zhil'tsova, I. G.; Polupanova, L. I.; Shmariovich, E. M.; Perlina, S. A. Physico-chemical conditions of uranyl-arsenate mineralization. *Litol. Polez. Iskop.* **1987**, No. 3, 44−54.
(60) Morosin, B. Hydrogen uranyl phosphate tetrahydrate, a hydrogen ion solid electrolyte. *Acta. Crystallogr. B. Struct. Sci. Cryst. Eng. Mater.* **1978**, *34* (12), 3732.
(61) Ivanova, A. G.; Budantseva, N. A.; Fedoseev, A. M. Synthesis, crystal structure, and properties of new actinide(VI) arsenates $(H_3O)[(AnO_2)(AsO_4)]{\cdot}3H_2O$ (An = U, Np, Pu). *Radiochemistry* **2017**, *59* (2), 119−123.
(62) Shilton, M. G.; Howe, A. T. Rapid H^+ conductivity in hydrogen uranyl phosphate-A solid H^+ electrolyte. *Mater. Res. Bull.* **1977**, *12* (7), 701−706.
(63) Benjamin, M. M.*Water Chemistry*; McGraw-Hill: Boston, 2002.

https://doi.org/10.1021/acs.est.2c06648
Environ. Sci. Technol. 2023, 57, 255−265

(64) Zhang, Y.; Navrotsky, A. Thermochemistry of rare-earth aluminate and aluminosilicate glasses. *J. Non. Cryst. Solids.* **2004**, *341* (1−3), 141−151.
(65) Forray, F. L.; Smith, A.M.L.; Navrotsky, A.; Wright, K.; Hudson-Edwards, K.A.; Dubbin, W.E. Synthesis, characterization and thermochemistry of synthetic PbAs, PbCu and PbZn jarosites. *Geochim. Cosmochim. Acta* **2014**, *127*, 107.
(66) Grenthe, I.; Fuger, J.; Konings, R. J. M.; Lemire, R. J.; Muller, A. B.; Gregu, C. N.-T.; Wanner, H.Chemical Thermodynamics 1: Chemical Thermodynamics of Uranium; North-Holland Elsevier Science: New York, 1992.
(67) Kubatko, K. A.; Helean, K. B.; Navrotsky, A.; Burns, P. C. Thermodynamics of uranyl minerals: Enthalpies of formation of rutherfordine, UO_2CO_3, andersonite, $Na_2CaUO_2(CO_3)_3(H_2O)_5$, and grimselite, $K_3NaUO_2(CO_3)_3H_2O$. *Am. Mineral.* **2005**, *90* (8−9), 1284.
(68) Robie, R. A.; Hemingway, B. S.; Fisher, J. R.Thermodynamic properties of minerals and related substances at 298.15 K and 1 bar (10^5 pascals) pressure and at higher temperatures. *U.S. Geological Survey Bulletin 1452*, 1978.

https://doi.org/10.1021/acs.est.2c06648
Environ. Sci. Technol. 2023, 57, 255−265